Intracrystalline Structure of Molecular Mercury Halide Intercalated in High-T_c Superconducting Lattice of $Bi_2Sr_2CaCu_2O_y$

Jin-Ho Choy,* Seong-Ju Hwang, and Nam-Gyu Park

Contribution from the Department of Chemistry, Center for Molecular Catalysis, Seoul National University, Seoul 151-742, Korea

Received June 12, 1996[⊗]

Abstract: X-ray absorption spectroscopic studies have been systematically carried out for the new high-T_c superconducting intercalation compounds, $(HgX_2)_{0.5}Bi_2Sr_2CaCu_2O_y$ (X = Br and I), with a hybridized crystal lattice consisting of superconducting layer and insulating one. From the Hg L_{III}-edge EXAFS analysis, it is found for the first time that the intercalated mercuric halide is stabilized as a linear molecule with the bond distance (Hg−X) of 2.46 Å for the $HgBr_2$ intercalate and 2.65 Å for the HgI_2 one, respectively. These are cross-confirmed not only by micro-Raman studies but also by one-dimensional electron density mapping based on (00*l*) X-ray reflections, which is well consistent with the EXAFS fitting results. The present I L_I- and Br K-edge XANES results indicate a partial electron transfer from the host lattice of $Bi_2Sr_2CaCu_2O_y$ to the intercalant HgX_2 layer with the partial oxidations of Bi_2O_2 and CuO_2 layers. And the latter was also observed clearly from the Bi L_{III}-edge XANES and Cu K-edge EXAFS analyses, which are in good agreement with the I L_I- and Br K-edge XANES results. It is, therefore, concluded that the charge transfer between host and guest is mainly responsible for the T_c evolution upon intercalation, and the T_c of this compound is surely related to the variation of hole concentration rather than electronic coupling along the *c*-axis.

Introduction

The idea of introducing foreign atoms, molecules, and ions into two-dimensional solid lattice opened a new field, intercalation chemistry, which has been recently extended to the high-T_c superconducting materials. An exciting and profitable feature of intercalation reaction is that guest and host experience some degree of perturbation in their physical and chemical properties. In this respect, its application to high-T_c superconductors provides an effective method not only to engineer the physical properties of host superconductor but also to investigate the mechanism responsible for high-T_c superconductivity and to develop new superconducting materials and devices.[1−19]

Previously we have performed systematic studies on the iodine intercalated $Bi_2Sr_2CaCu_2O_y$ and $Bi_{2-x}Pb_xSr_2Ca_2Cu_3O_y$ compounds and found that the guest iodine plays a role as an electron acceptor, that is, Lewis acid.[7−9] Based on this finding, an attempt has been made to intercalate various guest species with Lewis acidity. Recently we have successfully developed a new type of high-T_c superconducting compounds of M−X−Bi−Sr−Ca−Cu−O (M = Hg, Ag, and X = Br, I) where a superconducting layer and an insulating/superionic conducting one are regularly interstratified.[1−6] Among these new series of intercalates, the mercuric halide derivatives have been expected to be good model compounds for studying the high-T_c superconductivity of layered copper oxides, because they are chemically and crystallographically well-defined, except that their basal expansion upon intercalation becomes almost twice as large as that of the iodine intercalate. Although it is well expected that the electronic coupling between the adjacent blocks would be minimized in these intercalates due to their large increase of basal spacing, their superconducting properties remain unchanged but with a slightly depressed T_c. Such a result could not be understood on the viewpoint of interblock coupling scheme.[14,20] In order to understand the relation between T_c and lattice expansion or T_c and hole concentration as well as the effect of intercalation upon the geometric and

* To whom all correspondence should be addressed. FAX: (82) 2-872-9864. TEL: (82) 2-880-6658. E-mail: jhchoy@alliant.snu.ac.kr.

[⊗] Abstract published in *Advance ACS Abstracts,* January 15, 1997.

(1) Choy, J.-H.; Park, N.-G.; Hwang, S.-J.; Kim, D.-H.; Hur, N. H. *J. Am. Chem. Soc.* **1994**, *116*, 11564−11565.

(2) Choy, J.-H.; Park, N.-G.; Hwang, S.-J.; Khim, Z.-G. *J. Phys. Chem.* **1996**, *100*, 3873−3878.

(3) Choy, J.-H.; Kim, D.-K.; Park, N.-G.; Kim, D.-H.; Hwang, S.-J.; Hwang, S.-H.; Hur, N. H. *Physica C* **1994**, *235*−240, 1023−1024.

(4) Choy, J.-H.; Park, N.-G.; Kim, Y.-I.; Hwang, S.-H; Lee, J.-S.; Yoo, H.-I. *J. Phys. Chem.* **1995**, *99*, 7845−7848.

(5) Choy, J.-H.; Park, N.-G.; Hwang, S.-J.; Kim, Y.-I. *Synth. Metals* **1995**, *71*, 2055−2056.

(6) Choy, J.-H.; Park, N.-G.; Kim, Y.-I.; Kim, C.-H. *Eur. J. Solid State Inorg. Chem.* **1995**, *t32*, 701−709.

(7) Choy, J.-H.; Kang, S.-G.; Kim, D.-H.; Hwang, S.-J.; Itoh, M.; Inaguma, Y.; Nakamura, T. *J. Solid State Chem.* **1993**, *102*, 284−287.

(8) Choy, J.-H.; Hwang, S.-J.; Kim, D.-H.; Park, H.-H. *Synth. Metals* **1995**, *71*, 1589−1590.

(9) Choy, J.-H.; Kim, D.-K.; Kang, S.-G.; Kim, D.-H.; Hwang, S.-J. In *Superconducting Materials*; Etourneau, J., Torrance, J.-B., Yamauchi, H., Eds.; IITT-International: Paris, 1993; p 329.

(10) Subramanian, M. A. *J. Solid State Chem.* **1994**, *110*, 193−195.

(11) Huang, T.; Itoh, M.; Yu, J.; Inaguma, Y.; Nakamura, T. *Phys. Rev. B* **1994**, *49*, 9885−9890.

(12) Xiang, X.-D.; Mckernan, S.; Vareka, W.-A.; Zettl, A.; Corkill, J.-L.; Barbee III, T.-W.; Cohen, M.-L. *Nature* **1990**, *348*, 145−147.

(13) Xiang, X.-D.; Zettl, A.; Vareka, W.-A.; Corkill, J.-L.; Barbee III, T.-W.; Cohen, M. L. *Phys. Rev. B* **1991**, *43*, 11496−11499.

(14) Xiang, X.-D.; Vareka, W.-A.; Zettl, A.; Corkill, J.-L.; Barbee III, T. W.; Cohen, M.-L.; Kijima, N.; Gronsky, R. *Science* **1991**, *254*, 1487−1489.

(15) Xiang, X.-D.; Vareka, W.-A.; Zettl, A.; Corkill, J.-L.; Cohen, M.-L. *Phys. Rev. Lett.* **1992**, *68*, 530−533.

(16) Ma, J.; Alméras, P.; Kelley, R.-J.; Berger, H.; Margaritondo, G.; Umezawa, A.; Cohen, M.-L.; Onellion, M. *Physica C* **1994**, *227*, 371−376.

(17) Faulques, E.; Russo, R.-E. *Solid State Commun.* **1992**, *82*, 531−535.

(18) Huong, P.-V.; Verma, A.-L. *Phys. Rev. B* **1993**, *48*, 9869−9872.

(19) Trodahl, H.-L.; Pooke, D.; Gainsford, G.-J.; Kishio, K. *Physica C* **1993**, *213*, 427−432.

(20) Wheatley, J. M.; Hsu, T. C.; Anderson, P. W. *Nature* **1988**, *333*, 121.

S0002-7863(96)01993-2 CCC: $14.00

electronic structures of host and guest, the chemical bonding nature and crystal structure of these intercalates should be systematically investigated. However, the conventional spectroscopic method such as X-ray photoelectron spectroscopy is not so appropriate to probe the bulk electronic structure of the intercalation compounds whose surface might be easily contaminated from the reactant. Moreover, it is difficult to determine the in-plane crystal structure by means of X-ray diffraction (XRD) due to their high anisotropic nature. In this regard, X-ray absorption spectroscopy is the most powerful way of providing not only an electronic structural information of a specific absorbing atom (X-ray absorption near edge structure: XANES) but also a local structural one on the neighboring atoms of an absorber (extended X-ray absorption fine structure: EXAFS).[21−26]

In this work, we have performed the curve fitting analysis to the Hg L_{III}-edge EXAFS spectra in order to precisely determine the intracrystalline structure of the intercalated mercuric halides which is very important in understanding how they are stabilized in the $Bi_2Sr_2CaCu_2O_y$ lattice as well as in studying the anisotropic physical properties of the intercalation compounds.

The K- and L_I-edge XANES studies for halogen have been also made to probe orbitals with *p* character which are the primary orbitals interacting with host lattice. Among the various features in the K- and L_I-edge spectra, the white line, corresponding to the transition from the 1s (or 2s) level to unoccupied *n*p state above the Fermi level, yields a direct measure on the degree of charge transfer between host lattice and guest molecule. Information on the bonding state of guest molecules is very helpful in understanding the origin of T_c evolution upon intercalation and also for the further synthesis of new intercalation compounds, since it reveals the driving force of intercalating HgX_2 into Bi−Sr−Ca−Cu−O superconductor.

In addition to the XANES studies on the halogen K- and L_I-edges, the Bi L_{III}- and Cu K-edge XANES and EXAFS spectra have been also analyzed for the pristine and its intercalates in order to understand a relationship between the variation of electronic structure of CuO_2 layer and the T_c depression upon intercalation. This is thought to be very important in that it is quite difficult to examine the sole effect of a change in hole concentration with respect to T_c, since the conventional methods for controlling the oxidation state of copper, such as the substitution of aliovalent cation and the adjustment of oxygen content, usually induce the other contributing factors to the T_c evolution such as a structural phase transition and a phase separation.[27−29] Furthermore, on the basis of these XAS results, a role of Bi_2O_2 layer as a charge reservoir for the superconductive CuO_2 layer can be examined because the intercalated mercuric halides would perturb Bi_2O_2 layer mainly without any significant changes in other layers.[30,31]

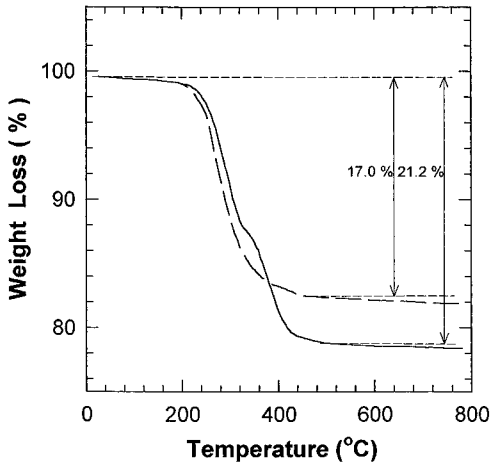

Figure 1. Thermogravimetric curves for $(HgBr_2)_{0.5}Bi_2Sr_2CaCu_2O_y$ (dashed lines) and $(HgI_2)_{0.5}Bi_2Sr_2CaCu_2O_y$ (solid lines). Samples are heated under ambient atmosphere at the rate of 10 °C/min.

Experimental Section

Sample Preparation and Characterization. The polycrystalline sample of $Bi_2Sr_2CaCu_2O_y$ was prepared by the conventional solid state reaction as follows: at first, the powder reagents of Bi_2O_3, $SrCO_3$, $CaCO_3$, and CuO were mixed with a molar ratio of Bi:Sr:Ca:Cu = 2:1.5:1.5:2 and calcined at 800 °C for 12 h in air, and then, the prefired material was pressed into 13 mm disk-shaped pellets and finally sintered at 860 °C for 40 h with intermittent grindings. On the other hand, the single-crystalline $Bi_2Sr_2CaCu_2O_y$ sample was synthesized by the traveling-solvent floating-zone method. Raw materials of Bi_2O_3, $Sr(NO_3)_2$, $CaCO_3$, and CuO powder were used in a molar ratio of Bi:Sr:Ca:Cu = 2.2:1.8:1:2 for the feed rod and 2.4:1.5:1:1.8 for the solvent one, respectively.

The intercalation of HgX_2 (X = Br and I) was performed by heating the vacuum sealed tube containing the pristine $Bi_2Sr_2CaCu_2O_y$ single crystals or polycrystals with 5 equiv HgX_2 per formula unit of host samples.[1] Especially, on HgI_2 intercalation, 1 mol of free iodine ($P(I_2) \cong 1$ atm) should be added as a transporting agent to complete the intercalation reaction. The first staged HgX_2 intercalates of polycrystalline $Bi_2Sr_2CaCu_2O_y$ were easily obtained by a short heat treatment (4−6 h) at 230−240 °C, whereas the intercalation of $HgBr_2$ into the single-crystalline host compound required a prolonged heating for more than 5 days. And moreover, an attempt to intercalate HgI_2 into the single crystal of $Bi_2Sr_2CaCu_2O_y$ compound was proved to be unsuccessful. A difficulty in intercalating into the single crystal is obviously attributed to its longer diffusion path and poorer capability for a large elastic deformation.

The formation of first staged intercalates was confirmed by XRD measurements using Ni-filtered Cu Kα radiation with a graphite diffracted beam monochromator. According to the least square fitting analysis, the increases of basal spacing upon intercalation were determined to be ∼12.6 Å for $(HgBr_2)_{0.5}Bi_2Sr_2CaCu_2O_y$ and ∼14.3 Å for $(HgI_2)_{0.5}Bi_2Sr_2CaCu_2O_y$, those which correspond to the lattice expansion of ∼6.30 Å for the former and ∼7.15 Å for the latter per each mercuric halide layer, respectively. Especially, the XRD pattern for the well-oriented $HgBr_2$ intercalate of single-crystalline host compound, where 14 (00*l*) reflections can be clearly observed, enabled us to precisely calculate one-dimensional electron density along the *c*-axis.

Thermogravimetric analysis (TGA) was carried out for the intercalates in the temperature range of 20−800 °C using DuPont 2000 thermal analysis station in order to confirm the reversibility of intercalation reaction and to determine the amount of guest species introduced into host lattice. According to the XRD patterns for the samples after TGA, it was found that the pristine $Bi_2Sr_2CaCu_2O_y$ phase was restored due to the disintercalation of HgX_2, indicating the reversibility of reaction. As shown in Figure 1, the intercalated mercuric halides are completely disintercalated below 500 °C, suggestive of a weak interaction between

(21) Choy, J.-H.; Kim, D.-K.; Hwang, S.-H; Park, J.-C. *J. Am. Chem. Soc.* **1995**, *117*, 7556−7557.
(22) Choy, J.-H.; Kim, D.-K.; Hwang, S.-H.; Demazeau, G. *Phys. Rev. B* **1994**, *50*, 16631−16639.
(23) Park, N.-G.; Cho, S.-W.; Kim, S.-J.; Choy, J.-H.; *Chem. Mater.* **1996**, *8*, 324−326.
(24) Choy, J.-H.; Yoon, J.-B.; Kim, D.-K.; Hwang, S.-H. *Inorg. Chem.* **1995**, *34*, 6524−6531.
(25) Choy, J.-H.; Kim, D.-K.; Demazeau, G.; Jung, D.-Y. *J. Phys. Chem.* **1994**, *98*, 6258−6262.
(26) Choy, J.-H.; Kim, D.-K.; Hwang, S.-H.; Demazeau, G.; Jung, D. Y. *J. Am. Chem. Soc.* **1995**, *117*, 8557−8566.
(27) Jorgensen, J. D.; Beno, M. A.; Hinks, D. G.; Soderholm, L.; Volin, K. J.; Hitterman, R. L.; Grace, J. D.; Schuller, I. K.; Segre, C. U.; Zhang, K.; Kleefisch, M. S. *Phys. Rev. B* **1987**, *36*, 3608−3616.
(28) Mitzi, D. B.; Lombardo, L. W.; Kapitulnik, A; Laderman, S. S.; Jacowitz R. D. *Phys. Rev. B* **1990**, *41*, 6564−6572.
(29) Maeda, A.; Hase, M.; Tsukada, I.; Noda, K.; Takebayashi, S.; Uchinokura K. *Phys. Rev. B* **1990**, *41*, 6418−6434.
(30) Mattheiss, L.-F.; Hamann, D.-R. *Phys. Rev. B* **1988**, *38*, 5012−5015.
(31) Pickett, W.-E. *Rev. Mod. Phys.* **1989**, *61*, 433−512.

Table 1. Observed and Calculated (in Parentheses) Weight Percents of Each Element in $HgBr_2$ and HgI_2 Intercalated $Bi_2Sr_2CaCu_2O_y$

element	X = Br	X = I
Hg	10.44 (9.60)	9.10 (9.18)
X	7.69 (7.65)	12.80 (11.62)
Bi	39.59 (40.00)	38.13 (38.28)
Sr	10.77 (12.58)	11.17 (12.04)
Ca	5.41 (5.75)	5.66 (5.51)
Cu	12.16 (12.16)	11.32 (11.64)
O	13.94 (12.26)	11.82 (11.73)

host lattice and guest molecule. The total weight losses were determined to be 17.0% for the $HgBr_2$ intercalate and 21.2% for the HgI_2 one, respectively, those which were in excellent agreement with the calculated values of $(HgBr_2)_{0.5}Bi_2Sr_2CaCu_2O_y$ (17.3%) and $(HgI_2)_{0.5}Bi_2Sr_2CaCu_2O_y$ (20.8%), respectively. The stoichiometries obtained from TGA were also confirmed by electron probe microanalysis (repeated five times), where the average atomic ratio among Hg, X, and Bi was estimated to be 0.5:1:2 in both compounds, as summarized in Table 1.

The evolution of superconductivity upon intercalation was examined by both dc magnetic susceptibility and resistivity measurements. Dc magnetic susceptibilities were measured as a function of temperature with a superconducting quantum interference device (SQUID) magnetometer, where the applied magnetic field was 20 Oe. Temperature dependent resistivities were obtained using a conventional four probe method.

X-ray Absorption Measurement. X-ray absorption experiments were carried out with synchrotron radiation by using EXAFS facilities installed at the beam lines 7C and 10B in the Photon Factory (National Laboratory for High Energy Physics, Tsukuba) operated at 2.5 GeV, 260−370 mA. Samples were finely ground, mixed with boron nitride (BN) in an appropriate ratio, and pressed into pellets, in order to obtain an optimum absorption jump ($\Delta\mu t \approx 1$) enough to be free from the thickness and pin-hole effects.[32,33] All the present spectra were obtained at room temperature in a transmission mode using gas-ionization detectors with a spacing of ∼0.4 eV for the XANES region and ∼1.5 eV for the EXAFS one. The silicon (311) channel-cut monochromator was used for the Cu K-, Hg L_{III}-, Bi L_{III}-, and Br K-edges, while silicon (111) double crystal monochromator, detuned to 60% of the maximum intensity to minimize the higher harmonics, was utilized for the I L_I-edge. To ensure the spectral reliability, much care was made to evaluate the stability of energy scale by monitoring the spectra of Cu metal and Bi_2O_3 for each measurement, and thus the edge positions were reproducible to better than 0.05 eV.

XANES and EXAFS Data Analysis. The data analysis for the present spectra was performed by the standard procedure as follows. The inherent background in the data was removed by fitting a polynomial to the pre-edge region and extrapolated through the entire spectrum, from which it was subtracted. The resulting spectra, $\mu(E)$, were normalized to an edge jump of unity for comparing the XANES features directly with one another. The absorption spectrum for the isolated atom, $\mu_0(E)$, was approximated by summing the cubic spline. The EXAFS oscillation, $\chi(E)$, was obtained as $\chi(E) = \{\mu(E) - \mu_0(E)\}/\mu_0(E)$. The data were converted to k space where the photoelectron wave vector k is defined as $k = 8\pi[2m_e(E - E_0)/h^2]^{1/2}$, where k is the wave vector, m_e is the electron mass, and E_0 is the threshold energy. The resulting $\chi(k)$ oscillation was weighted by a factor of k^3 to compensate the attenuation of EXAFS signal with increasing photon energy and Fourier transformed with a Hanning apodization function. In order to determine the structural parameters such as bond distance and coordination number, a nonlinear least square fitting procedure was carried out for the inverse Fourier transformed $k^3\chi(k)$ of the first shell in the Fourier transform by using the EXAFS formula on the basis of the plane wave single scattering description, which can be expressed as follows[34]

$$\chi(k) = S_0^2 \sum_i N_i F_i(k) \exp\{-2\sigma_i^2 k^2\} \exp\{-2R_i/\lambda(k)\} \sin\{2kR_i + \phi_i(k)\}/(kR_i^2)$$

where $F_i(k)$ is the back scattering amplitude from each of the N_i neighboring atoms at a R_i distance with a Debye−Waller factor of σ_i^2, S_0 is the amplitude reduction factor, $\phi_i(k)$ is the total phase shift, and $\lambda(k)$ is the photoelectron mean free path.

The curve fitting procedure was performed by using $F_i(k)$, $\phi_i(k)$, and $\lambda(k)$, theoretically calculated by a curved wave *ab initio* EXAFS code FEFF 5.[35] The refinements were based on the minimization of F factor, $F = [\sum\{\chi^3(\chi(k)_{cal} - \chi(k)_{exp})\}^2/(n-1)]^{1/2}$, where $\chi(k)_{exp}$, $\chi(k)_{cal}$, and n represent the experimental EXAFS oscillation, the fitted oscillation, and the number of data point, respectively.

Results and Discussion

Hg L_{III}-Edge XANES. Figure 2a,b represents the Hg L_{III}-edge spline spectra and their second derivatives for the HgX_2 intercalates and the reference HgX_2 compounds, respectively. The selection rule for photoelectric excitation in the dipolar approximation predicts that the transitions to final states with orbital angular momentum quantum number l_f, which is different from the initial state with l_i by ±1 unit, are allowed.[34] Since all the present compounds contain a Hg^{+II} ion with vacant 6s and 6d orbitals, not only the main-edge peaks corresponding to $2p_{3/2} \rightarrow 6d$ transition but also the pre-edge peak A corresponding to $2p_{3/2} \rightarrow 6s$ one is observed commonly for the references HgX_2 and the HgX_2 intercalates.[36] As can be seen clearly from the second derivatives, the intensity of the peak A is stronger for the HgX_2 intercalates than for the corresponding free HgX_2 compounds. According to the previous Hg L_{III}-edge XAS studies,[36,37] the intensity of this pre-edge peak decreases with an increase of coordination number around mercury ion, i.e., linear > tetrahedral > octahedral, which is due to a more Rydberg-like character of the excited orbitals for the higher coordination numbers. Therefore, an enhancement of the pre-edge peak A upon intercalation suggests strongly a change in local symmetry of mercuric halide.

Hg L_{III}-Edge EXAFS. Although the profile refinement technique is one of the most powerful ones to investigate the crystal structure of solids, it is very hard to apply it to the present HgX_2 intercalates, since they have to suffer from the severe elastic deformation upon intercalation leading to poorer crystallinity. In fact, there has been no diffraction refinement study for the previous intercalation compounds of $Bi_2Sr_2CaCu_2O_y$. In this respect, the EXAFS analysis has been performed especially for determining the intracrystalline structure of intercalant layer.

The k^3-weighted Hg L_{III}-edge EXAFS spectra for the HgX_2 intercalates and the unintercalated free HgX_2 compounds are shown in Figure 3a[38] and the corresponding Fourier transforms in the k range of 2.9−11.9 Å^{-1} in Figure 3b. The first peak in Fourier transforms is attributed to the mercury−halogen bonding pair. In contrast to a single peak in the Fourier transforms of the free $HgBr_2$ and the $HgBr_2$ intercalate, a doubly split feature is observed at around 2.0 and 2.6 Å in those of the free HgI_2

(32) Lytle, F. W.; van der Laan, G.; Greegor, R. B.; Larson, E. M.; Violet, C. E.; Wong, J. *Phys. Rev. B* **1990**, *41*, 8955−8963.

(33) Stern, E.-A.; Kim, K. *Phys. Rev. B* **1981**, *23*, 3781.

(34) Teo, B. K. *EXAFS: Basic Principles and Data Analysis*; Springer-Verlag: Berlin, 1986.

(35) Rehr, J.-J.; Mustre de Leon, J.; Zabinsky, S.-I.; Albers, R.-C. *J. Am. Chem. Soc.* **1991**, *113*, 5135−5140. Mustre de Leon, J.; Rehr, J.-J.; Zabinsky, S.-I.; Albers, R.-C. *Phys. Rev. B.* **1991**, *44*, 4146−4156. O'Day, P.-A.; Rehr, J.-J.; Zabinsky, S.-I.; Brown, G.-E., Jr. *J. Am. Chem. Soc.* **1994**, *116*, 2938−2949.

(36) Åkesson, R.; Persson, I.; Sandstrom, M.; Wahlgren, U. *Inorg. Chem.* **1994**, *33*, 3715−3723.

(37) Yamamura, T.; Watanabe, T.; Kikuchi, A.; Ushiyama, M.; Kobayashi, T.; Hirota, H. *J. Phys. Chem.* **1995**, *99*, 5525−5531.

(38) As shown in Figure 3a, the amplitude of Hg L_{III}-edge EXAFS oscillation is not so high enough for both intercalates, which is clearly due to the quite small contents of mercury in the unit formula of intercalates $(HgX_2)_{0.5}Bi_2Sr_2CaCu_2O_y$. But the present data are surely the best available for these samples, because we have carefully controlled the mixing ratio of sample and boron nitride (BN) in order to obtain the optimum edge jump.

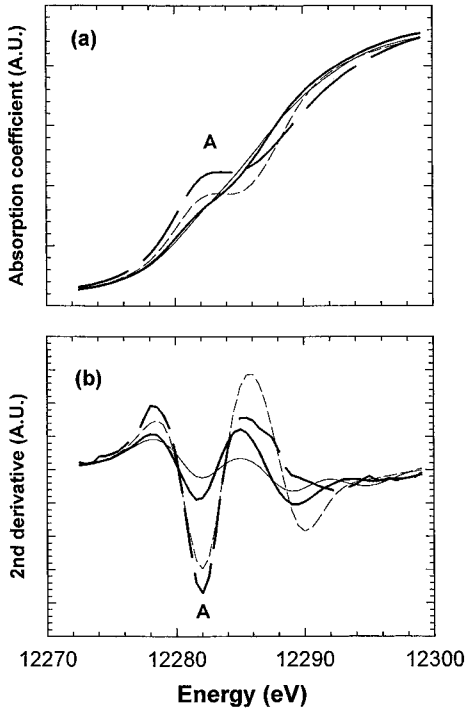

Figure 2. (a) Hg L_{III}-edge XANES spectra for HgI_2 (lightface solid lines), $(HgI_2)_{0.5}Bi_2Sr_2CaCu_2O_y$ (boldface solid lines), $HgBr_2$ (lightface dashed lines), and $(HgBr_2)_{0.5}Bi_2Sr_2CaCu_2O_y$ (boldface dashed lines) and (b) their second derivatives. The peak A corresponds to $2p_{3/2} \rightarrow 6s$ transition.

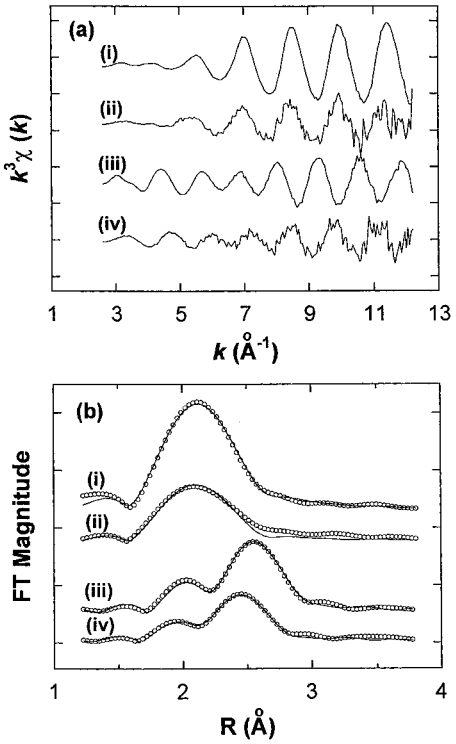

Figure 3. (a) Experimental k^3-weighted Hg L_{III}-edge EXAFS spectra and (b) their Fourier transforms of (i) $HgBr_2$, (ii) $(HgBr_2)_{0.5}Bi_2Sr_2CaCu_2O_y$, (iii) HgI_2, and (iv) $(HgI_2)_{0.5}Bi_2Sr_2CaCu_2O_y$. The solid lines and empty circles represent the fitted and experimental data, respectively.

and the HgI_2 intercalate. Such a peak splitting is attributed to the Ramsauer−Townsend resonance which occurs generally in the backscattering amplitude of heavy atom with high atomic number.[39] The first coordination shell of mercury−halogen bond was isolated by inverse Fourier transformation to k space. The resulting $k^3\chi(k)$ Fourier filtered EXAFS oscillations are

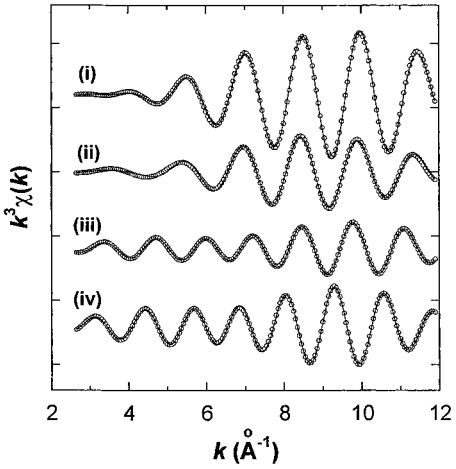

Figure 4. Comparison of the fitted spectra with the experimental data of (i) $HgBr_2$, (ii) $(HgBr_2)_{0.5}Bi_2Sr_2CaCu_2O_y$, (iii) HgI_2, and (iv) $(HgI_2)_{0.5}Bi_2Sr_2CaCu_2O_y$. The solid lines and empty circles represent the fitted and experimental data, respectively.

Table 2. Results of Nonlinear Least Square Curve Fitting for the First Shell of Hg L_{III}-Edge EXAFS Spectra

	parameter		
compound	bond distance (Å)	coordination no.	Debye−Waller factor (10^{-3} Å^2)
$HgBr_2$	2.45_9	$2 + 4^a$	3.09
$(HgBr_2)_{0.5}Bi_2Sr_2CaCu_2O_y$	2.46_2	1.85_7	6.41
HgI_2	2.76_0	4^a	7.27
$(HgI_2)_{0.5}Bi_2Sr_2CaCu_2O_y$	2.64_7	2.06_6	6.86

[a] The coordination numbers of reference HgX_2 were fixed to the crystallographic value with a view to determining the amplitude reduction factor. According to the previous crystallographic studies, the reference HgI_2 has a HgI_4 tetrahedron, while the $HgBr_2$ solid has a linear $HgBr_2$ with more distant four coordination shell. The curve fitting analyses for these references were performed to the first coordination shell data.

shown in Figure 4, and the curve fittings were carried out to them in order to determine the structural parameters such as coordination number (N), bond length (R(Hg−X)), and Debye−Waller factor (σ^2). As shown in Figure 4, the amplitudes of EXAFS oscillation are commonly decreased for both HgX_2 intercalates with respect to the corresponding free HgX_2 molecules. In general, there are two effects on the amplitude in k space; one is the effect of neighboring atoms where the signal tends to increase in the entire k range with increasing the coordination number, and the other is the effect of the Debye−Waller factor, whose increase attenuates the amplitude at high k region.[34] A closer inspection reveals that the amplitude of the free HgI_2 is decreased uniformly over the entire k range upon intercalation, indicating a decrease in coordination number, whereas an amplitude depression upon $HgBr_2$ intercalation is more prominent in high k region than in low k one, reflecting an increase in the Debye−Waller factor. It is also observed that the oscillation frequency is larger for the HgI_2 intercalate than for the free HgI_2, while there is little difference between the $HgBr_2$ intercalate and the free $HgBr_2$. This implies that the (Hg−I) bond distance is remarkably decreased upon intercalation in contrast to (Hg−Br) one. The best fitting results to the first coordination shell are compared to the experimental spectra in Figures 3b and 4 and the fitted structural parameters are summarized in Table 2. Since the coordination number obtained from the fitting analysis corresponds to the product (S_0^2N) of coordination number (N) and amplitude reduction factor (S_0^2),[34]

(39) Mott, N.-F; Massey, H.-S.-W. *The Theory of Atomic Collisions*; Clarendon Press: Oxford, 1965.

it is necessary to get the knowledge of amplitude reduction factor for a specific absorber−scatterer pair, prior to determining the exact coordination number. In the present analysis, the amplitude reduction factors obtained from the free HgX_2 references (0.80_3 and 0.72_1 for $HgBr_2$ and HgI_2, respectively) were used to calculate the coordination number of mercury in the corresponding HgX_2 intercalates, those which were found to be two for both intercalates. According to the previous crystallographic studies,[40] the HgI_2 solid has a HgI_4 tetrahedron, while the $HgBr_2$ solid has a linear local symmetry around mercury with more distant coordination shells. In contrast, these mercuric halides have a linear two-coordinated structure in vapor state commonly.[40−42] Therefore, the present fitting results indicate that the mercuric halide molecule intercalated into host lattice is stabilized as a linear molecule as in the gaseous state. To our knowledge, these HgX_2 intercalates are the first examples of linear molecular salts of $HgBr_2$ and HgI_2 stabilized in the solid lattice. In order to certificate this peculiar linear symmetry, we have attempted alternatively to fit them on the basis of the local symmetry of mercuric halide in solid state. However, those gave significantly poorer fits.

As listed in Table 2, the bond distances of 2.45_9 Å for the free $HgBr_2$ and 2.76_0 Å for the free HgI_2 show only a small difference from the previously reported crystallographic values,[40] which confirms the reliability of the present EXAFS analyses. In the case of the intercalates, the (Hg−X) bond distances were found to be $2.46_2 \pm 0.00_7$ Å for the $HgBr_2$ intercalate and $2.64_7 \pm 0.00_6$ Å for the HgI_2 one, which are surely larger than those for the HgX_2 vapors (d(Hg−Br) = 2.40 Å and d(Hg−I) = 2.568 Å).[42,43] A small but distinct increase of (Hg−X) bond distance upon HgX_2 intercalation is attributed to the chemical interaction between halide layer and Bi_2O_2 one, which is surely absent in the vapor state. On the basis of the Fajan's rule,[44] the chemical bonding between bismuth and halogen is expected to be stronger for the HgI_2 intercalate than for the $HgBr_2$ one, because the iodine has a greater polarizability with respect to the bromine. As a result, the competing (Hg−X) bond is suggested to be more weakened and elongated upon HgI_2 intercalation compared to $HgBr_2$ one, which is well consistent with the present EXAFS results where an increase of bond distance upon intercalation, $\Delta d = d$(Hg−X; in the intercalate) − d(Hg−X; in the vapor), is determined to be 0.06 Å for the $HgBr_2$ intercalate and 0.08 Å for the HgI_2 one.

We can obtain further information on the local crystal structure of mercury from Debye−Waller factor (σ^2), which corresponds to the mean square relative displacement (MSRD) of the equilibrium of the (Hg−X) bond distance due to the vibrational disorder and/or due to the static one.[45,46] It is well-known that a longer bond distance gives rise to a larger Debye−Waller factor due to a stronger thermal vibration, and the presence of static disorder owing to the defect structure or multiple bond distances also induces an enhancement of this factor. As presented in Table 2, this factor was found to be larger for the $HgBr_2$ intercalate than for the reference $HgBr_2$. Since the bond distances of (Hg−Br) are almost the same for both compounds implying the similar contribution of thermal vibration, an increase of σ^2 upon $HgBr_2$ intercalation is attributed to an enhanced static disorder which is originated from the local defect structure of intercalant layer. In contrast to the $HgBr_2$ intercalate, the Debye−Waller factor becomes smaller for the HgI_2 intercalate relative to the reference HgI_2, which is in good agreement with a decrease of bond distance from 2.78 Å of the free HgI_2 to 2.65 Å of the HgI_2 intercalate, resulting in a depression of thermal vibration.

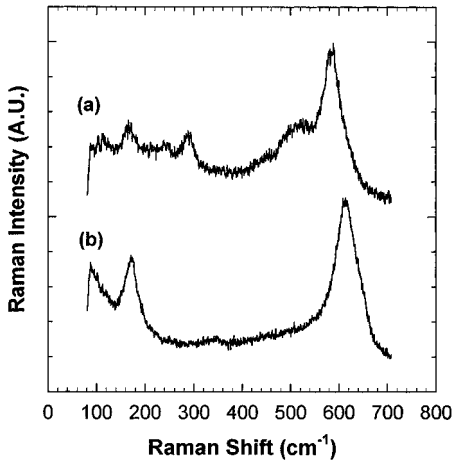

Figure 5. The polarized Raman spectra for the $HgBr_2$ intercalate of single crystalline $Bi_2Sr_2CaCu_2O_y$ compound with (a) $z(x\bar{x})\bar{z}$ and (b) $x(z\bar{z})\bar{x}$ scattering geometry.

Micro-Raman Analysis. Further evidence on the linear HgX_2 molecule in between Bi_2O_2 layers can be obtained from the polarized Raman spectroscopic studies. Figure 5a,b represents the polarized Raman spectra of the $HgBr_2$ intercalate of $Bi_2Sr_2CaCu_2O_y$ single-crystal with $z(x\bar{x})\bar{z}$ and $x(z\bar{z})\bar{x}$ scattering geometry, respectively. The present spectra exhibit unique spectral features which are quite different from those of the pristine,[47] indicating the influence of intercalation on the phonon modes of the host lattice. Since the Raman peaks whose frequencies are higher than ∼250 cm^{-1} are related to the vibrations of oxygen, the lower frequency ones should be assigned to the vibrations of heavier elements such as mercury and halogen. The group theoretical calculation for the triatomic linear structure predicted that the linear $HgBr_2$ molecule has only one Raman active vibration (ν_1), which was observed at 225 cm^{-1} for the vapor species.[48] Moreover, in the case of the $HgBr_2$ intercalate, this vibration is expected to have a considerable spectral activity for both $z(x\bar{x})\bar{z}$ and $x(z\bar{z})\bar{x}$ scattering geometries, since the $HgBr_2$ molecule is stabilized inbetween (Bi−O) double layer with a considerable tilting angle to the basal plane.[1] As expected, a characteristic peak corresponding to this symmetric stretching (ν_1) vibration is observed at 170 cm^{-1} commonly for both scattering geometries, indicating the linear local structure of intercalated $HgBr_2$. Its frequency decrease upon intercalation is well consistent with the Hg L_{III}-edge EXAFS fitting results where the (Hg−Br) bond is elongated after intercalation due to its interaction with host lattice. The detailed and complete assignments for all the Raman peaks will be reported elsewhere.

Structure Modeling and 1-D Fourier Map. The structural model of the HgX_2 intercalates has been suggested on the basis of the EXAFS fitting results (Figure 6). To confirm the reliability of this structure, one-dimensional electron density maps along the c-axis obtained in two different ways are compared; one was calculated from the (00l) reflection intensities in the XRD pattern for the well-oriented $HgBr_2$ intercalate of $Bi_2Sr_2CaCu_2O_y$ single crystal, and the other was obtained from the structural factor based on the present structural model.

(40) Wells, A.-F. *Structural Inorganic Chemistry*; Clarendon Press: Oxford, 1984.
(41) W. Klemperer, *J. Chem. Phys.* **1956**, *25*, 1066.
(42) Gregg, A. H.; Hampson, G. C.; Jenkins, G. I.; Jones, P. L. F. *Trans. Faraday. Soc.* **1937**, *33*, 852.
(43) Spiridonov, V. P.; Gershikov, A. G.; Butaev, B. S. *J. Mol. Struct.* **1979**, *52*, 53.
(44) Huheey, J.-E.; Keiter, E.-A.; Keiter, R.-L. *Inorganic Chemistry*, 4th ed.; HarperCollins College Publishers: 1993.
(45) Tranquada, J. M.; Ingalls, R. *Phys. Rev. B* **1981**, *28*, 3520.
(46) Shem, T. K. *Acc. Chem. Res.* **1986**, *19*, 99.
(47) Liu, R; Klein, M. V.; Han, P. D.; Payne, D. A. *Phys. Rev. B* **1992**, *45*, 7392−7396.
(48) Janz, G. J.; James, D. W. *J. Chem. Phys.* **1963**, *38*, 902.

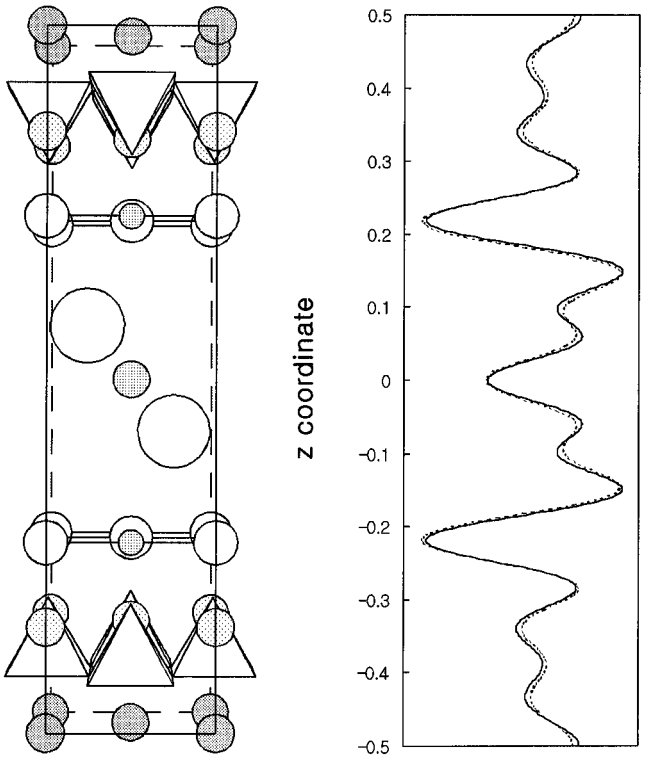

Figure 6. One-dimensional electron density mappings along the *c*-axis of $(HgBr_2)_{0.5}Bi_2Sr_2CaCu_2O_y$, together with the structural model. The dotted and solid lines represent the calculated data based on the intensities of the (00*l*) reflections in the XRD pattern of the $HgBr_2$ intercalate of $Bi_2Sr_2CaCu_2O_y$ single-crystal and those on the basis of the structural parameters calculated from the present structural model, respectively.

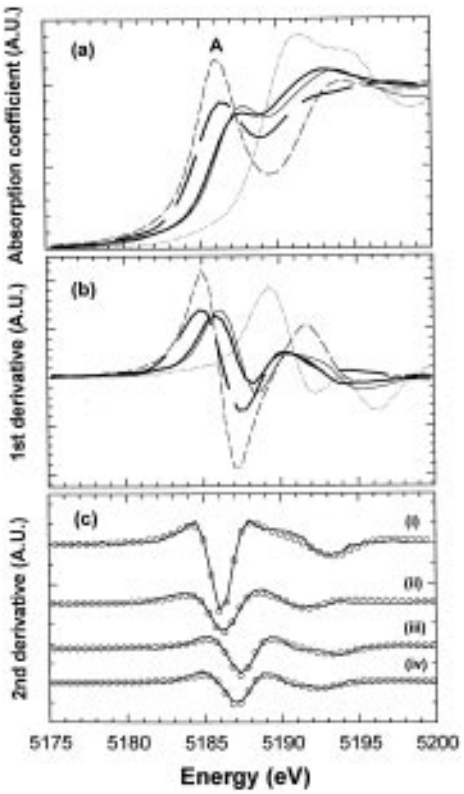

Figure 7. (a) I L_I-edge XANES spectra for I_2 (lightface dashed lines), $IBi_2Sr_2CaCu_2O_y$ (boldface dashed lines), KI (dotted lines), HgI_2 (lightface solid lines), and $(HgI_2)_{0.5}Bi_2Sr_2CaCu_2O_y$ (boldface solid lines) and (b) their first derivatives. (c) Comparison of the calculated spectra (empty circles) with the experimental ones (solid lines) of the I L_I-edge second derivative spectra for (i) I_2, (ii) $IBi_2Sr_2CaCu_2O_y$, (iii) HgI_2, and (iv) $(HgI_2)_{0.5}Bi_2Sr_2CaCu_2O_y$. The peak A corresponds to 2s → 5p transition.

As shown in Figure 6, there is an excellent accordance between both electron density maps, which confirms the reliability of the present structural model and the presence of linear HgX_2 molecule inbetween (Bi−O) double layer.[49] From this result, the tilting angle of $HgBr_2$ molecular axis was determined to be 65° with respect to the *c*-axis.

I L_I-Edge XANES. Figure 7 shows the I L_I-edge XANES spectra and their first and second derivatives for the HgI_2 intercalate and the free HgI_2, together with the iodine intercalate, I_2, and KI for comparison. All spectra except for KI exhibit a pre-edge peak A (so-called "white line" type feature) in 5185−5188 eV region, assigned to the transition from 2s core level into 5p state above the Fermi energy level (E_F). It is clearly seen that the peak A has a considerable intensity for the neutral I_2 molecule with a hole in the 5p state, whereas it disappears for ionic compound such as KI where the final 5p state is fully occupied. In contrast to KI, HgI_2 even with formal I^- state, however, exhibits a small but distinct pre-edge peak, which is attributed to the formation of partially empty 5p state due to a strong covalent mixing between Hg 6s orbital and I $5p_z$ one.[50] This is well expected from high polarizabilities of soft I^- and Hg^{2+} ion with an electronic configuration of $[Xe]4f^{14}5d^{10}6s^0$, where d and f electrons shield the nucleus poorly, compared to the K^+ ion with a $[Ne]3s^23p^64s^0$ electronic configuration. In this context, a remarkable decrease in the peak intensity upon iodine intercalation has been interpreted as a proof of negatively charged iodine species in the $Bi_2Sr_2CaCu_2O_y$ lattice, which is in good accordance with the other spectroscopic studies.[7−11,17−19] In the case of HgI_2 intercalation, the intensity of pre-edge peak A is also depressed upon intercalation, which indicates that the intercalant HgI_2 layer receives the electron from host lattice. The change in the oxidation state of iodine can be also checked out from the variation of energy difference between the white line peak and the second absorption one at about 5190 eV corresponding to the transition to the unbound continuum state. As shown in the figure, there is a shift of continuum peak to lower energy side both for the iodine intercalate and for the HgI_2 one, compared to the corresponding unintercalated species. From the peak position in the first-derivative spectra, the transition energy of 2s → 5p (E_{WL}) and 2s → continuum state (E_C) are determined as listed in Table 3. According to the previous study on the iodine intercalated C_{60},[23] the energy difference between both peaks ($\Delta E = E_{WL} - E_C$), associated with the energy gap between the highest occupied level and the unbound continuum state, is inversely proportional to the electron density of antibonding state. Therefore, the observed decrease in ΔE upon HgI_2 intercalation confirms that the vacant I 5p state of HgI_2 is partially occupied by the electron from host lattice.

In order to get the quantitative information on charge transfer, the area of the pre-edge peak A has been calculated by least square fitting analysis to the second derivative spectra with a Lorentzian function (Figure 7c).[51] Since the second derivation makes the amplitude corresponding to the transition to continuum state almost negligible, the fitting procedure to the second derivative spectra has an advantage in that the number

(49) The obtained atomic *z*-coordinates are listed as follows: Hg (0), Br (0.481), Bi (0.228, 0.216), Sr (0.344), Cu (0.411), Ca (0.5), O_{Bi} (0.222), O_{Sr} (0.3), and O_{Cu} (0.428). The incommensurate modulation in Bi_2O_2 layer was taken into account by placing the bismuth ion in two different sites. The theoretical X-ray diffraction pattern based on the present structural model is well consistent with the experimental one.

(50) Turner, D. E.; Harmon, B. N. *Phys. Rev. B* **1989**, *40*, 10516−10522.

(51) The unit of peak area is expressed as a product of energy (eV) and peak intensity which is normalized to a continuum region.

Table 3. Edge Energies of the I L_I-Edge XANES Spectral Feature and Peak Areas of White Line (WL) for the Iodine and HgI_2 Intercalated $Bi_2Sr_2CaCu_2O_y$ and the Unintercalated Iodine and HgI_2

compound	E_{WL} (eV)[a]	E_C (eV)[a]	area of WL[b]	ΔE (eV)
I_2	5184.6	5191.7	6.32	7.1
$IBi_2Sr_2CaCu_2O_y$	5184.7	5190.3	4.68	5.6
HgI_2	5186.2	5190.8	3.60	4.6
$(HgI_2)_{0.5}Bi_2Sr_2CaCu_2O_y$	5185.8	5190.2	2.98	4.4

[a] Edge energies were determined from the peak positions in the first derivative spectra. [b] Peak areas of pre-edge were calculated by fitting the second derivative spectra to Lorentzian functions.

of variable is reduced by excluding contribution due to the transition to the continuum state, and, therefore, we get a physically meaningful evolution in the edge spectral features.[32] For this reason, this fitting method has been extensively used for its simplicity and accuracy compared to the fitting analysis to the spline spectra.[25,26,52,53] The best-fitting results are compared with the experimental spectra in Figure 7c and listed in Table 3. The density of unoccupied 5p state can be obtained from the relative area of a Lorentzian function, which is reduced to 74% for the iodine intercalate compared to that for I_2 molecule. Assuming the linear relationship between the peak area and the density of vacancy, this result indicates an electron transfer of ca. 0.3 per iodine atom, which is well consistent with the presence of I_3^- ion as assigned by Raman spectroscopy.[17−19] In contrast to a remarkable reduction of peak area upon iodine intercalation, the HgI_2 one gives rise to only a slight peak depression from 3.60 eV for the free HgI_2 to 2.98 eV for the HgI_2 intercalate, which corresponds to an electron transfer of 0.1 e^- per formula unit.[54] However, it should be noted that the white line area in the XANES spectra does not necessarily represent the statistical vacancy of unoccupied *p* states because of various factors that influence the peak area such as the thickness effect and covalent bonding character.[55,56] But the present fitting results show clearly that the degree of electron transfer is smaller for the HgI_2 intercalate than for the iodine one, which is well correlated with a less decreased T_c of the former with respect to the latter.

Br K-Edge XANES. The Br K-edge XANES analysis was also made to investigate the evolution of electronic structure of bromine upon $HgBr_2$ intercalation. Even though a small energy difference between the Br K-edge (13470 eV) and the Bi L_{III}-one (13426 eV) results in a significant perturbation each other, an attempt was made to separate the Br K-edge contribution by subtracting the Bi L_{III}-edge spectrum of HgI_2 intercalate from the raw spectrum. Such an attempt can be reasonably accepted since both HgX_2 intercalates are expected to have a similar chemical environment of bismuth, and, moreover, the Bi L_{III}-edge EXAFS signal in this region is much weaker compared to the Br K-edge XANES one. The resulting Br K-edge spectra and their second derivatives for the $HgBr_2$ intercalate and the free $HgBr_2$ are shown in Figure 8 (parts a and b, respectively). As observed in the I L_I-edge XANES spectra, the white line peak A, corresponding to the transition from 1s level to 4p state,

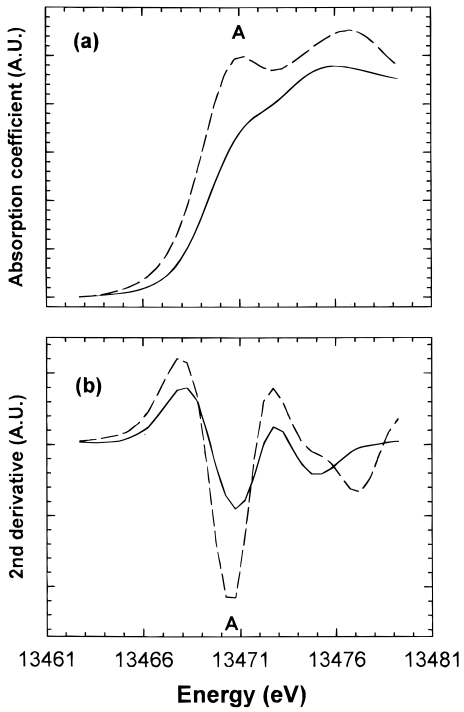

Figure 8. (a) Br K-edge XANES spectra for $HgBr_2$ (dashed lines) and $(HgBr_2)_{0.5}Bi_2Sr_2CaCu_2O_y$ (solid lines), and (b) their second derivatives. The peak A corresponds to 1s → 4p transition.

is depressed upon intercalation, indicating a partial filling of Br 4p state due to the electron transfer from host lattice. This is also cross-confirmed by a variation in ΔE ($= E_{WL} - E_C$), which is decreased from 5.0 eV of the free $HgBr_2$ to 4.3 eV of the $HgBr_2$ intercalate. But an attempt has not been made to calculate the peak area quantitatively because the uncertainty originated from the subtracting treatment makes the fitting result less meaningful.

From the above I L_I- and Br K-edge XANES results, it is obvious that the intercalated HgX_2 molecules receive a small fraction of electron from the host lattice, resulting in a negatively charged state of $(HgX_2)^{\delta-}$. From the viewpoint of electronic structure, it implies that the σ^* orbital of HgX_2 unit forms a band, and the bottom of this band lies slightly below the Fermi level. Such a band structure of intercalated HgX_2 species is interpreted as a result of an electrostatic interaction between bismuth cation and halide anion in the interlayer space of two-dimensional $Bi_2Sr_2CaCu_2O_y$ lattice, which gives rise to a weakening of covalency in the competing (Hg−X) bond. Due to this bond weakening, the antibonding σ^* orbital of HgX_2 unit should be less destabilized, and, therefore, this band can dip below the Fermi level. In fact, the above interpretation is supported not only by Hg L_{III}-edge EXAFS analysis but also by micro-Raman spectroscopic studies. This negatively charged state of intercalated HgX_2 allows us to understand how the linear two-coordinated mercuric halide molecules can be stabilized in the solid lattice. According to the *ab initio* psuedopotential study for the binary mercury compounds,[57] the electrostatic factor was found to be most important in determining the coordination number for the compounds with quite electronegative groups such as the halides, even though the traditional $s-d_z^2$ hybridization argument may be useful for ligands like hydride and alkyl groups. And it was also claimed that the relativistic contraction of the mercury 6s orbital reduces the charge separation between metal and ligands and thus also decreases the low-order multipole interactions between the HgX_2 molecules, which makes two-coordinated structure energetically

(52) George, G. N.; Cleland, W. E., Jr.; Enemark, J. H.; Smith, B. E.; Kipke, C. A.; Roberts, S. A.; Cramer, S. P. *J. Am. Chem. Soc.* **1990**, *112*, 2541.

(53) Lytle, F. W.; Greegor, R. B. *Appl. Phys. Lett.* **1990**, *56*, 192.

(54) The peak area of HgI_2 corresponds to the presence of 0.56 hole per each I 5p state due to hybridization of (Hg−I) bond. Using the Pauling's formula for (a−b) bond ionicity (*I*) calculation, $I = 1 - \exp[-1/4(\chi_a - \chi_b)^2]$, the ionic character of (Hg−I) in this compound is determined to be 43.7%, which is in good agreement with the hole density obtained from XANES spectra.

(55) Lytle, F. W. *In Applications of Synchrotron Radiation*; Winick, H., et al., Eds; Wiley-Interscience: New-York, 1988; pp 211−253.

(56) de Groot, F. M. F.; Fuggle, J. C.; Thole, B. T.; Sawatzky, G. A. *Phys. Rev. B* **1990**, *41*, 928; **1990**, *42*, 5459.

(57) Kaupp, M.; Schnering, H. G. *Inorg. Chem.* **1994**, *33*, 2555−2564.

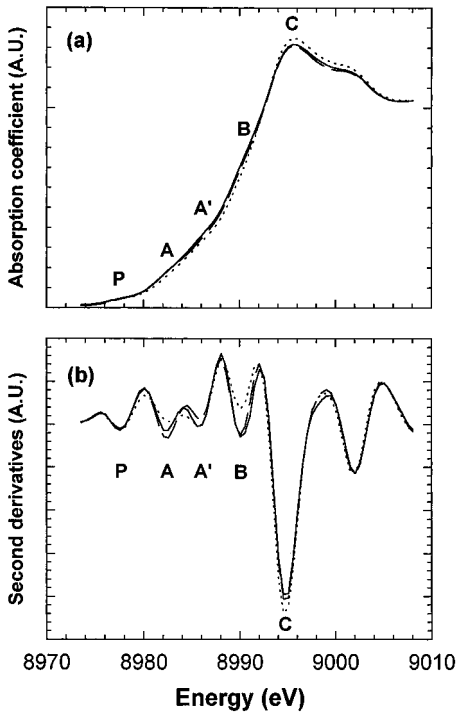

Figure 9. (a) Cu K-edge XANES spectra for $Bi_2Sr_2CaCu_2O_y$ (solid lines), $(HgBr_2)_{0.5}Bi_2Sr_2CaCu_2O_y$ (dotted lines), and $(HgI_2)_{0.5}Bi_2Sr_2CaCu_2O_y$ (dashed lines) and (b) their second derivatives. The peaks P, A, B, C and A′ correspond to $1s \rightarrow 4d$, $1s \rightarrow 4p_\pi(d^{10}\underline{L})$, $1s \rightarrow 4p_\pi(d^9)$, $1s \rightarrow 4p_\sigma(d^9)$, and $1s \rightarrow 4p_\sigma(d^9\underline{L})$ transitions, respectively.

favorable. In the case of the HgX_2 intercalates, although the relativistic contraction of mercury 6s orbital remains unchanged before and after intercalation, the electron transfer from host lattice to halogen layer decreases the electron withdrawal power of halogen, which gives rise to a decrease of the charge separation between mercury and halogen and, therefore, results in a weakening of the intermolecular interaction between HgX_2 molecules. Moreover, an increase of negative charge in halogen enhances the repulsive force between the adjacent halide anions. For these reasons, the unique coordination number of two is more favorable in the intercalates than the higher coordination number.

Cu K-Edge XANES and EXAFS. Figure 9a,b represents the Cu K-edge XANES spectra for the pristine and its HgX_2 intercalates and their second derivatives, respectively. All the present spectra show a small pre-edge peak (denoted as P), which is assigned to the transition from core 1s level to unoccupied 3d state. Even though it is not allowed by electronic dipolar selection rule, $\Delta l = \pm 1$, the pre-edge peak A could be observed either due to a quadrupole-allowed transition and/or due to a mixing of 4p and 3d states.[22] In the main-edge region, three kinds of features are observed commonly for all the present compounds, those which are characteristics of divalent cuprate compound. According to our previous XAS study on the cuprate compounds with various valence states and local symmetries of copper,[22] the main-edge features A and B are attributed to the transition from 1s orbital to the out-of-plane $4p_\pi$ one, whereas the feature C is ascribed to the in-plane $4p_\sigma$ orbital transition. Since the coulombic energy between Cu 1s hole and 3d electron is much larger than the ligand to metal charge transfer energy, the lower energy peak A is assigned to the transition to the shake down final state of $1s^13d^{10}4p_\pi^1\underline{L}$ ($\underline{L}$ represents a hole in the ligand shell) where an electron in oxygen 2p orbital is transferred to the copper 3d one.[22,58] In addition to these peaks, the spectral feature corresponding to the transition from the $1s^23d^8$ state to the $1s^13d^94p_\sigma^1\underline{L}$ one was also observed at 8985.7 eV (denoted as A′), which has been revealed as an indicator for the presence of Cu^{+III} ion.[21,22] In fact, this peak has been effectively applied for investigating the oxidation state of copper in chemically and electrochemically prepared $La_2CuO_{4.08}$.[21]

On the basis of the above assignments, we have examined the effect of intercalation on CuO_2 layer by comparing the Cu K-edge XANES derivative spectra of the pristine $Bi_2Sr_2CaCu_2O_y$ and its HgX_2 intercalates. However, there is no prominent change in the edge energy and the peak intensity including the peak A′ upon intercalation, suggesting that the modification of electronic structure in CuO_2 layer is too weak to be observed. In fact, the Cu K-edge XANES cannot reflect sensitively such a small change, since it does not probe the orbital with *d* character that is directly involved in the chemical bonding. It is, however, expected that such a small change in electronic structure can be detected by measuring the (Cu−O) bond distances. Even though the crystal structure of copper oxide superconductors has been mainly investigated by X-ray diffraction method,[59] it is not easy to measure precisely the copper−oxygen bond distance in the intercalate because of the strong orientation effect as well as the low X-ray scattering factor of oxygen. In this respect, the determination of (Cu−O) bond distance by means of the Cu K-edge EXAFS would be effective since the first shell for the nearest neighbor of oxygen around copper ion is well separated from the other distant shells.[60−62]

The k^3-weighted EXAFS spectra for the pristine and its HgX_2 intercalates are presented in Figure 10a, and the corresponding Fourier transforms are presented in the *k* range of 2.6−12.8 $Å^{-1}$ in Figure 10b. The first prominent peak in Fourier transforms is assigned to the in-plane and out-of-plane (Cu−O) pairs which are overlapped due to their similar bond distance, which is followed by the peaks corresponding to the Cu−Ca, Sr shells, and the Cu−Cu one.[60−62] The first shell due to (Cu−O) bond was isolated by inverse Fourier transformation to *k* space. The resulting $k^3\chi(k)$ Fourier filtered EXAFS oscillations are shown in Figure 11, and the curve fittings were carried out to them in order to determine the (Cu−O) bond distances. In the fitting procedure, only the bond distance and the Debye−Waller factor were allowed to be refined, but the coordination number was fixed to a crystallographic value in order to avoid an inaccuracy probably caused by its strong correlation with Debye−Waller factor. The best fitting results to the first coordination shell are compared with the experimental spectra in Figure 11, and the fitted structural parameters are listed in Table 4. As shown in the table, the out-of-plane ($Cu-O_{Sr}$) bond distance is rather decreased upon intercalation, whereas the in-plane ($Cu-O_p$) one is not significantly changed. Although it is well-known that the latter is closely related to the hole concentration of CuO_2 layer,[63] its variation has been found to be quite minute even with a considerable change in hole concentration of CuO_2 layer and T_c. Previously M. H. Whangbo *et al.*[63] showed that the T_c depression of more than 30 K (much larger than the T_c variation upon HgX_2 intercalation) induces only a slight decrease in ($Cu-O_p$) bond distance of smaller than 0.005 Å, which is surely below the detection limit of EXAFS

(58) Kosugi, N.; Kondoh, H.; Tajima, H.; Kuroda, H. *Chem. Phys.* **1989**, *135*, 149−160.
(59) Yvon, K.; Francois, M. *Z. Phys. B* **1989**, *76*, 413−444.
(60) Koizumi, A.; Maruyama, H.; Yamazaki, H.; Maeda, H.; Ishii, T.; Miura, Y.; Takada, J. *Physica C* **1992**, *190*, 338−344.
(61) Lottici, P. P.; Antonioli, G.; Licci, F. *Physica C* **1988**, *152*, 468−474.
(62) DiMarzio, D.; Wiesmann, H.; Chen, D. H.; Heald, S. M. *Phys. Rev. B* **1990**, *42*, 294−300.
(63) Whangbo, M. H.; Kang, D. B.; Toradi, C. C. *Physica C* **1989**, *158*, 371−376.

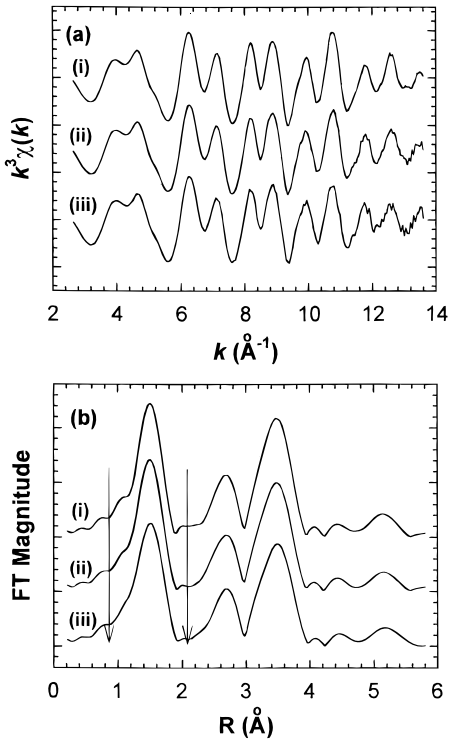

Figure 10. (a) Experimental k^3-weighted Cu K-edge EXAFS spectra and (b) their Fourier transforms for (i) the pristine $Bi_2Sr_2CaCu_2O_y$, (ii) $(HgBr_2)_{0.5}Bi_2Sr_2CaCu_2O_y$, and (iii) $(HgI_2)_{0.5}Bi_2Sr_2CaCu_2O_y$. The range over which the Fourier filtering has been made is shown by the arrows.

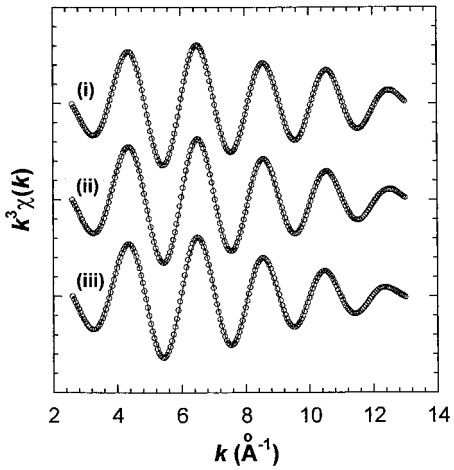

Figure 11. Comparison of the fitted spectra with the experimental data for (i) the pristine $Bi_2Sr_2CaCu_2O_y$, (ii) $(HgBr_2)_{0.5}Bi_2Sr_2CaCu_2O_y$, and (iii) $(HgI_2)_{0.5}Bi_2Sr_2CaCu_2O_y$. The solid lines and empty circles represent the fitted and experimental data, respectively.

analysis. Therefore, it is not surprising that we could not observe any change in the bond distance of ($Cu-O_p$) before and after intercalation. In contrast to the in-plane (Cu−O) bond distance, the out-of-plane (Cu−O) one reflects sensitively even a small increase in hole concentration of CuO_2 layer.[28,64] In this context, the observed decrease of ($Cu-O_{Sr}$) bond distance upon intercalation can be interpreted as a clear evidence of the oxidation of CuO_2 layer. Such a change in (Cu−O) layer is suggested to be either due to a charge transfer between host and guest and/or due to a change in oxygen content induced by the heat-treatment during intercalation reaction. But, according to the previous study on the oxygen loss effect,[65] it is clear that the annealing in a vacuum sealed tube at the low temperature of 230−240 °C does not induce any significant change in the oxygen content of host lattice and T_c. Therefore, the observed remarkable change in ($Cu-O_{Sr}$) bond is completely attributed to a charge transfer between guest HgX_2 layer and CuO_2 one along the bonds of $Bi-O_{Sr}-Cu$. And it was also found that the effect of intercalation on the bond distance is more prominent for the HgI_2 intercalate than for the $HgBr_2$ one, which is well consistent with ΔT_c upon intercalation. It is, therefore, concluded that the charge transfer plays an important role in the T_c change upon intercalation.

Bi L_{III}-Edge XANES. Figure 12a represents the Bi L_{III}-edge XANES spectra for the pristine and its HgX_2 intercalates. As mentioned above, the electric dipole selection rule allows the transition not only to the 6d final state but also to the 6s one. In fact, three broad peaks, indicated as A, B, and C, are observed in all the present spectra, and their positions are summarized in Table 5. Among them, the pre-edge peak A is assigned to the $2p_{3/2} \rightarrow 6s$ transition on the basis of previous XANES study on the PbO_2.[66−68] And the main-edge peaks B and C in the high energy side are attributed to the transition to the 6d final state. Since the bismuth ion in the $Bi_2Sr_2CaCu_2O_y$ superconductor is stabilized in the octahedral environment,[59] the degenerated 6d orbitals are split into $6d_{t2g}$ and $6d_{eg}$ levels. Thus, the lower energy peak B and the higher one C are assigned to $2p_{3/2} \rightarrow 6d_{t2g}$ transition and $2p_{3/2} \rightarrow 6d_{eg}$ one, respectively.[67,69]

On the basis of the above assignments, the effect of intercalation on Bi_2O_2 layer has been precisely investigated by examining the first and second derivatives of the pristine and its HgX_2 intercalates. As shown in the first derivatives (Figure 12b), the edge energy is increased upon HgX_2 intercalation, indicative of the oxidation of bismuth ion. The amount of edge shift was determined to be 0.05 eV for the $HgBr_2$ intercalate and 0.10 eV for the HgI_2 one. According to the previous study on the Bi^{+III} and Bi^{+V} containing compounds,[69] it was found that the increase of edge energy of 2.2 eV corresponds to the enhancement of formal valence from 3.2 to 5. On the basis of this result, a partial increase of Bi oxidation state upon intercalation was evaluated to be 0.04 for the $HgBr_2$ intercalate and 0.08 for the HgI_2 one. And it was also found from the second derivatives (Figure 12c) that the energy difference between the peaks B and C is diminished upon intercalation. Even though their energy difference is not exactly equal to the ground state crystal field parameter ($10Dq$), the peak splitting is surely proportional to the strength of crystal field.[25,26] Therefore, the observed decrease in energy difference reflects the weakening of crystal field around Bi upon intercalation, which is thought to be originated from the following two effects. One is the effect of introducing the guest molecules in between the Bi_2O_2 double layer in which one of axial oxygen in the BiO_6 octahedron is replaced by bromine or iodine. Since the electronegativities of halogens are quite smaller than that of oxygen, the strength of crystal field around the bismuth ion is decreased upon intercalation. And the other is the effect of increasing the ($Bi-O_{Sr}$) bond distance which is well expected from the Cu K-edge EXAFS results. Because the apical oxygen is coordinated to copper ion on one direction and to bismuth ion on the other one,[59] a remarkable shortening of the (Cu−

(64) Shimakawa, Y.; Kubo, Y.; Manako, T.; Igarashi, H.; Izumi, F.; Asano, H. *Phys. Rev. B* **1990**, *42*, 10165−10171. Martin, C.; Maignan, A.; Labbe, Ph.; Charadon, J.; Hejtmanek, J.; Raveau, B. *Chem. Mater.* **1995**, *7*, 1414; A. Sequeira, A.; Yakhmi, J. V. *Studies of High Temperature Superconductors*; Nova Science Publishers: H. Y.; 1993; Vol. 11, pp 107−129.

(65) Nagoshi, M.; Suzuki, T.; Fukuda, Y.; Terashima, K.; Nakanishi, Y.; Ogita, M.; Tokiwa, A.; Syono, Y.; Tachiki, M. *Phys. Rev. B* **1991**, *43*, 10445−10450.

(66) Rao, K. J.; Wong, J. *J. Chem. Phys.* **1984**, *81*, 4832−4843.

(67) Studer, F.; Bourgault, D.; Martin, C.; Retoux, R.; Michael, C.; Raveau, B.; Dartyge, E.; Fontaine, A. *Physica C* **1989**, *159*, 609−615.

(68) Faiz, F.; Jennings, G.; Campuzano, J.-C.; Alp, E.-E.; Yao, J.-M.; Saldin, D.-K.; Yu, J.-J. *Phys. Rev. B* **1994**, *50*, 6370−6374.

(69) Retoux, R.; Studer, F.; Michael, C.; Raveau, B.; Fontaine, A.; Dartyge, E. *Phys. Rev. B* **1990**, *41*, 193−199.

Table 4. Results of Nonlinear Least Square Curve Fitting for the First Shell of Cu K-Edge EXAFS Spectra for the Pristine $Bi_2Sr_2CaCu_2O_y$ and Its HgX_2 Intercalates

parameter		$Bi_2Sr_2CaCu_2O_y$	$(HgBr_2)_{0.5}Bi_2Sr_2CaCu_2O_y$	$(HgI_2)_{0.5}Bi_2Sr_2CaCu_2O_y$
R	(Cu−O_p)	1.90_1 Å	1.90_0 Å	1.90_7 Å
	(Cu−O_{Sr})	2.36_4 Å	2.34_8 Å	2.33_8 Å
σ^2	(Cu−O_p)	$3.2_0 \times 10^{-3}$ Å^2	$4.0_6 \times 10^{-3}$ Å^2	$4.8_5 \times 10^{-3}$ Å^2
	(Cu−O_{Sr})	$4.7_0 \times 10^{-3}$ Å^2	$4.4_1 \times 10^{-3}$ Å^2	$5.7_2 \times 10^{-3}$ Å^2
CN[a]	(Cu−O_p)	4	4	4
	(Cu−O_{Sr})	1	1	1

[a] The coordination numbers were fixed to crystallographic values due to their strong correlation with Debye−Waller factor.

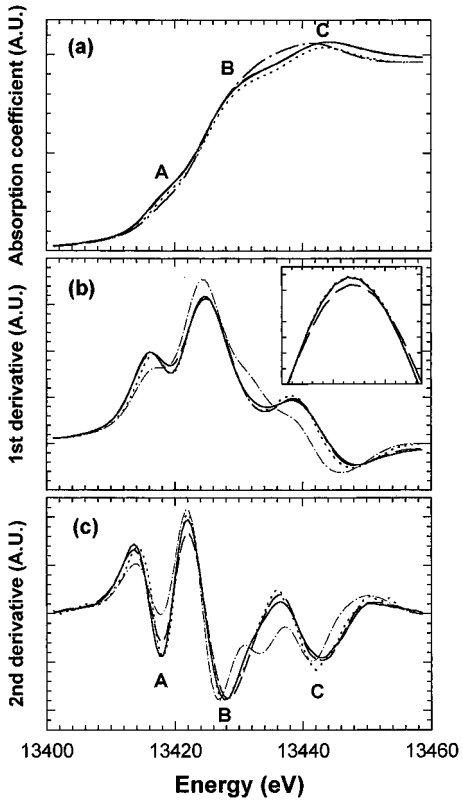

Figure 12. (a) Bi L_{III}-edge XANES spectra for $Bi_2Sr_2CaCu_2O_y$ (solid lines), $(HgBr_2)_{0.5}Bi_2Sr_2CaCu_2O_y$ (dotted lines), $(HgI_2)_{0.5}Bi_2Sr_2CaCu_2O_y$ (dashed lines), and Bi_2O_3 (dotted-dashed lines) and their (b) first and (c) second derivatives. The peaks A, B, and C correspond to $2p_{3/2} \rightarrow 6s$, $2p_{3/2} \rightarrow 6d_{t2g}$, and $2p_{3/2} \rightarrow 6d_{eg}$ transitions, respectively. The inset in (b) represents the enlarged first derivatives in the energy range of 13422−13427.4 eV.

Table 5. Peak Energies of the Bi L_{III}-Edge XANES Spectral Feature for the Pristine $Bi_2Sr_2CaCu_2O_y$ and Its HgX_2 Intercalates

compound	A (eV)[a]	B (eV)[a]	C (eV)[a]	C − B (eV)[a]
$Bi_2Sr_2CaCu_2O_y$	13417.7	13428.0	13442.9	14.9
$(HgBr_2)_{0.5}Bi_2Sr_2CaCu_2O_y$	13418.0	13428.0	13442.4	14.4
$(HgI_2)_{0.5}Bi_2Sr_2CaCu_2O_y$	13417.8	13428.5	13442.9	14.4

[a] Peak energies were determined from the peak positions in the second derivative spectra.

O_{Sr}) bond distance induces an increase of the competing (Bi−O_{Sr}) bond distance and thus a weakening of crystal field around Bi.

From the present Cu K- and Bi L_{III}-edge XANES and EXAFS results, it is clear that both the CuO_2 layer and Bi_2O_2 one are partially oxidized upon intercalation due to the charge transfer between host and guest. Such a result can be suggested as an evidence on the internal redox mechanism in these compounds, since a positive charge from the intercalant HgX_2 layer can be delocalized between both layers through this mechanism. However, even though this self-doping mechanism in the pristine compound was suggested by the band calculations,[30,31] X-ray absorption spectroscopic studies,[69] photoemission experiments,[70,71] and, moreover, the synthesis of high-T_c superconducting $Bi_2Sr_2CaCu_2O_8$ compound without excess oxygen,[72] the other band calculation based on the modulated structure of Bi_2O_2 layer predicted that the bottom of the Bi 6p band lies more than 1 eV above the Fermi level, implying the internal charge transfer mechanism is not working in the pristine.[73] In this respect, the co-oxidation of CuO_2 and Bi_2O_2 layers upon intercalation might be related to the structural modification of (Bi−O) layer induced by introducing the foreign molecule into the interlayer space, which gives rise to the intersection of Bi 6p band with E_F.

Conclusion

In this work, we have elucidated for the first time that the intercalated mercuric halide is stabilized as a linear molecule as in the vapor state in between the two-dimensional solid lattice. And we have also found from the I L_I- and Br K-edge XANES studies that a small fraction of electron (≤ 0.1 e^- per unit formula of $Bi_2Sr_2CaCu_2O_y$) is transferred from the host lattice to the intercalated HgX_2 layer. In this respect, the intercalation reaction can be considered as a kind of Lewis acid−base reaction where the guest molecule acts as a Lewis acid, while the host lattice plays a role as a Lewis base. Therefore, the soft Lewis acid is proposed to be an appropriate candidate as a guest intercalating into the Bi−Sr−Ca−Cu−O superconductor with soft Lewis basicity. On the other hand, the present Cu K- and Bi L_{III}-edge XANES/EXAFS results reveal clearly the co-oxidation of CuO_2 and Bi_2O_2 layers upon intercalation through an internal redox mechanism of the host lattice, which is well consistent with the I L_I- and Br K-edge XANES results. It is, therefore, concluded that the charge transfer between host and guest is mainly responsible for the T_c evolution upon intercalation, and the T_c of this compound is surely related to the variation of hole concentration rather than electronic coupling along the *c*-axis.

Acknowledgment. This work was in part supported by the Ministry of Science and Technology for the high temperature superconductivity research and by the Korea Science and Engineering Foundation through the Center for Molecular Catalysis. Authors are grateful to Prof. M. Nomura for helping us to get the XAS data in the Photon Factory. S. J. Hwang is also grateful to the Korean Research Foundation for the scholarship.

JA961993X

(70) Böttner, R.; Schroeder, N.; Dietz, E.; Gerhardt, V.; Assmers, W.; Kowalewsi, J. *Phys. Rev. B* **1990**, *41*, 8679.

(71) Hillebrecht, F. V.; Fraxadas, J.; Ley, L.; Trodah, H. J.; Zaanen, J.; Braun, W.; Most, M.; Peterson, H.; Schaible, M.; Bourne, L. C.; Pinsukayama, P.; Zettl, A. *Phys. Rev. B* **1989**, *39*, 236.

(72) Pham, A. Q.; Maignan, A.; Hervieu, M.; Michel, C.; Provost, J.; Raveau, B. *Physica C* **1992**, *191*, 77. Krishinaraj, P.; Eror, N. G.; Balachandran, U. *Physica C* **1994**, *234*, 318.; Krishinaraj, P.; Lelovic, M.; Eror, N. G.; Balachandran, U. *Physica C* **1995**, *246*, 271.

(73) Ren, J.; Jung, D.; Whangbo, M. H.; Tarascon, J. M.; Le Page, Y.; Mckinnon, W. R.; Toradi, C. C. *Physica C* **1989**, *158*, 501−506.